Anal. Bioanal. Electrochem., Vol. 14, No. 5, 2022, 486-509

Analytical & Bioanalytical Electrochemistry

2022 by CEE
www.abechem.com

Full Paper

Thermodynamics Analysis and Optimization of a Novel Integrated System with PEM Fuel Cell, PV/Thermal Cells, and Membrane Distillation Unit for Power and Freshwater Production

Hamed Pourfarzad,[1] Mohammad Saremi,[2] Ramin Jazmi,[3] Saman Khadem Jafari,[4] and Ramin Badrnezhad[5,*]

[1]*Center of Excellence in Electrochemistry, University of Tehran, Tehran, Iran*
[2]*Department of Electrical Engineering, College of Technical and Engineering, West Tehran Branch Islamic Azad University, Tehran, P.O. Box 14687-6378, Iran*
[3]*Department of Mechanical Engineering, Tarbiat Modares University, Tehran, Iran*
[4]*Tarbiat Modares University, Department of Material Engineering, Tehran, P.O. Box 15875-4416, Iran*
[5]*Department of Chemistry and Chemical Engineering, Malek-Ashtar University of Technology, Tehran, P.O. Box 15875-1774, Iran*

*Corresponding Author, Tel.: +989393939207
E-Mail: Badrnezhad@yahoo.com

Received: 30 March 2022 / Received in revised form: 3 May 2022 / Accepted: 17 May 2022 / Published online: 31 May 2022

Abstract- In this paper, a novel integrated system for power generation and freshwater production is proposed. The system consists of Proton exchange membrane fuel cell (PEMFC), photovoltaic (PV) thermal cells and Proton exchange membrane electrolyzer (PEME) in addition to a membrane distillation (MD) system for freshwater production. The proposed system is assessed from thermodynamics viewpoints through first and second law analyses and the modeling and simulation of the subsystems are conducted in EES software to provide a comprehensive assessment concerning thermodynamic criteria. Simulation of each subsystem is validated by considering the reported data in the previous works. The proposed system is subsequently optimized via a multi-objective optimization method based on genetic algorithm. The results showed that PV cell temperature and PV area are the main influential parameters that can affect the power output and exergy efficiency. The optimization results show that at a well-balanced operating point, power and exergy efficiency would be 30 kW and 11.7%, respectively.

Keywords- Photovoltaic/Thermal cells; PEM Fuel Cell; PEM Electrolyzer; Membrane Distillation; Optimization

Nomenclature

A	Area (m^2)
C	Concentration
C_m	Membrane distillation coefficient (kg/m^2 s pa)
C_p	Heat capacity (kJ/kg K)
C_s	Salinity of water (%)
d	Mean pore diameter (m)
E	Voltage (V)
$\dot{E}$	Exergy rate (kW)
F	Faraday constant(C/mol)
G	Solar radiation (W/m^2)
ΔG	Gibbs energy change (kJ/kg)
H	Enthalpy (kJ)
h	heat transfer coefficient (W/m^2 K)
J_w	MD mass flux (kg/m^2 s)
J	Current density (A/m^2)
m	Mass flow rate (kg/s)
$\dot{N}$	Molar flow rate (mol/s)
p	Partial pressure
P	Power (kW)
Q	Heat load (kW)
q	heat load (kJ/kg)
R	Universal gas constant (J/mol K)
s	Specific entropy (kJ/kg K)
S	Mean free path of transferred gas molecule (m)
T	Temperature (K)
u	Speed (m/s)
U	Overall heat transfer coefficient (W/m^2 K)
V	Voltage (V)
x	Molar fraction
x_m	Membrane depth (m)

Greek letters

λ	Stoichiometric rate of air or H_2O content
η_{th}, η_{ex}	Thermal and exergy efficiency
η_{act}, η_{ohm}	Activation and ohmic overpotential (vol)
ε	Emissivity
k_B	Boltzmann constant (1.380622×10^{-23} J/K)

Subscripts, superscripts and abbreviations

a	Ambient
act	Activation
ch	Chemical
con	Convection
conc	Concentration
D	Destruction
ex	Exergy
g	glass
in	Inlet
MD	Membrane Distillation
Ner	Nernst
ohm	Ohmic
out	Outlet
PEMFC	Proton exchange membrane fuel cell
PEME	Proton exchange membrane electrolyzer
PVT	Photovoltaic/thermal
rad	Radiation
sat	Saturation
sol	Solar
th	Thermal

1. INTRODUCTION

Increasing energy demand made the utilization of energy storage systems an important issue [1-4]. Although one-third of the earth is covered by water, just 3% of it is drinkable water[5]. For 97% unpotable water, the Desalination technic used for continues removing salt from salty water and making it to appropriate for drinking [6]. For this purpose, the fuel cell is highlighted as a device to convert chemical energy into electricity which can be considered a sustainable alternative for fuel-based power plants [7]. Moreover, solar energy can play a pivotal role because of its huge potential in heat energy production. Integrating solar energy with fuel cells for providing electricity by heating energy of solar radiations in energy systems has been scrutinized by researchers and their technical features, challenges and trends extract.

Proton exchange membrane fuel cell performance based on thermodynamic and exergetic standpoints evaluated in some studies [8-10]. Yilanci [11] found that exergy and energy productivities of the plant increment with pressure by 15% and 23%. Also, anode stoichiometry optimization enhanced mentioned parameters by 14 and 17 percent. Regarding the huge potential of fuel cells for utilization in stationary and mobile energy plants, as well as in automotive, marine factories, or aerospace units. some studies established to evaluate PEMFC with PV energy systems [12-16]. For improving PV system efficiency, the application of nanofluid and PCM were studied [17,18]. PEMFC can be integrated with thermoelectric generator [19], PV and thermal plant, gas thermogeneration system [20], Reverse osmosis desalination and PV hybrid [12][21-24]. geothermal resources [25] or solar air preheating sub-system [26]. By integrating kalian generation systems with a desalination unit and solar flat plate collector (FPC) in a tri-generation energy system in HYSIS, MATLAB, and TRANSYS, 1869 kW electricity was achieved at 65194 kW heating load with 83.22 kg/s desalinated water. Total exergy and energy efficiencies of mentioned integrated systems are 90.04% and 44.64% [27].

Proton exchange membrane electrolyzer (PEME) split water molecules into hydrogen and oxygen molecule. Hydrogen gas has the highest energy gravimetric and is used in various applications. PEME device can integrate with PV cells for H_2 production [28,29], PVT and absorption chiller [30], PEMFC and CCHP [31], WHR and desalination (exergy and energy are 37.9% and 47.7%) [32]. CCHP unit with exergetic and thermal efficiencies 54.55% and 81.55% [33], PEMFC and PV cells at 20.4% and 21.8% energy and exergy efficiency [34]. From a exergoeconomic point of view, Saving thermal energy from heat generators (like waste heat of PV) with PCM or CO_2 gas may increase the efficiency of the systems [35-38]. Also, waste heat can be used in novel LCLG systems [39]. Results showed integration of PEME unit with other energy devices like PEMEFC and PC cells has higher energy and exergy efficiency. PEME devices can integrate with wind breakers to reduce the extra heat generated [40]. In addition to mentioned devices, it's found that membrane distillation technology has advantages

to RO like lower pressure and temperature, No need for electrical power. MD Device can integrate with PVT and PEMEFC cells for required freshwater [37,41].

According to the previous studies, the performance of the hybrid energy system coupling of MD with PEMFC system and the performance of the hybrid MD system with PV/Thermal cells [41] have been studied in separate researches, but So far, no study had been performed on the performance of the triple hybrid energy system consisting of MD, PEMFC and PV/Thermal cells, So in this study, for the first time, the combination of these three systems has been investigated.

To summarize, the objectives of this paper can be outlined as:

- To propose a novel configuration consisting of PVT cells, PEMFC, an electrolyzer, and an MD system for power and freshwater production
- To conduct thermodynamic analysis of the proposed system based on first and second laws
- To optimize the proposed configuration using a multi-objective genetic algorithm approach

2. EXPERIMENTAL

2.1. System description

The schematic of the proposed energy system has been shown in Figure 1. The proposed system consists of a PVT, a water electrolyzer(WE), a PEMFC unit, an MD unit, a reservoir tank, two electricity distributors (ED), and one tank for storing the salty water.

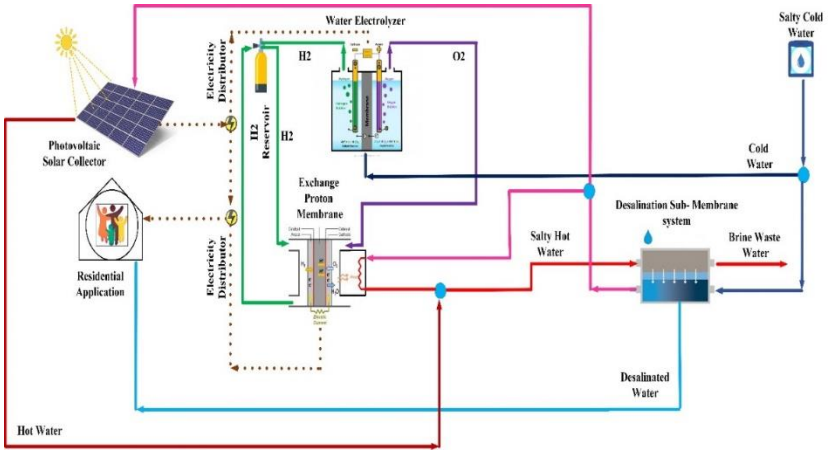

Figure 1. Schematic of proposed energy system

The system is designed to supply the electricity and freshwater demand of the residential application. In the first step, PVT converts the solar radiation into electricity and then the generated electricity is divided into two currents. The first one goes to the WE to generate

hydrogen and oxygen in electrolyze process, and the second one is transferred to the second ED. On the other hand, in the second ED current is mixed with the PEMFC's generated electricity, and goes to the network to respond to the electricity demand of the residential application. In the WE the water is split into oxygen and hydrogen by the electric current and in the electrolyzing process. Next, the generated hydrogen and oxygen are conducted into PEMFC to generate power and heat. Through the PEMFC, electric current and heat are produced in the proton exchange process between hydrogen and oxygen molecules. Regarding the point that the in the operation process of PEMFC heat is generated, to use the heating capacity of this energy, the desalination unit's inlet salty water is preheated by the mentioned heat. Next, the preheated salty water exiting from the PEMFC mixes with PVT's hot stream and goes to the desalination unit. In the MD sub-system, the required energy is provided by the hot stream. Freshwater is generated by the steam of salty water, and consequently, the salinity of outlet hot water increases. Finally, three flows exit from this sub-system: the first stream is the generated freshwater that goes to the residential application, the second is the brine wastewater with high salinity that is discharged to the environment and the third one is salty hot water that is returned to the solar collector to be heated again. Therefore, the process is completed and the desalinated water and generated electricity are transferred into the residential application to respond to the freshwater and energy demands.

2.2. Modeling

The whole modeling and simulation of the subsystems are conducted in EES software to provide a comprehensive assessment concerning thermodynamic criteria. For this purpose, energy and exergy balance relations are implemented in each subsystem. Here, we explain each employed subsystem briefly to help the readers replicate the results.

2.2.1. Energy analysis

2.2.2.1. PEMFC

The main reactions (Eq. 1-3) occurring in the PEMFCs are [42]:

$$\text{Anode side: } H_2 \rightarrow 2H^+ + 2e^- \quad (1)$$

$$\text{Cathode side: } 2H^+ + 2e^- + 0.5O_2 \rightarrow H_2O + \text{heat} \quad (2)$$

$$\text{Overall: } H_2 + 0.5O_2 \rightarrow H_2O + \text{heat} \quad (3)$$

In addition, reversible open-circuit voltage in the PEMFC can be represented by the Nernst equation (Eq. 4) [43]:

$$E_{Ner} = \frac{RT_{FC}}{n_e F} \ln\left(\frac{p_{H_2}\sqrt{p_{O_2}}}{p_{H_2O}^{sat}}\right) - \frac{\Delta G^0}{n_e F} \quad (4)$$

where ΔG^0 indicates the Gibbs free energy, and n_e denotes the electrons contributing to the reaction. T_{FC} is the cell temperature and p denotes partial pressure of the constituent.

Steam saturation pressure can be written as (Eq. 5) [44]:

$$\log_{10}(P_{H_2O}^{sat}) = -2.1794 + 0.02953T - 9.1837\times10^{-5}T^2 + 1.4454\times10^{-7}T^{-3} \quad (5)$$

in which, T denotes the operating temperature in °C (Eq. 6):

$$T = T_{FC} - 273.15 \quad (6)$$

In addition, partial pressure of oxygen and hydrogen respectively at the anode and cathode sides are given by (Eq. 7,8):

$$P_{O_2} = P\left\{1 - x_{H_2O}^{sat} - x_{N_2}^{channel}\, e^{\left(\frac{0.291I}{T_{FC}^{0.832}}\right)}\right\} \quad (7)$$

$$P_{H_2} = \left(0.5P_{H_2O}^{sat}\right)\left\{\frac{1}{e^{\left(\frac{1.653I}{T_{FC}^{1.334}}\right)} x_{H_2O}^{sat}} - 1\right\} \quad (8)$$

where (Eq. 8) I denote the current density and $x_{N_2}^{channel}$ is the molar fraction of N_2. $x_{H_2O}^{sat}$ is given by (Eq. 9):

$$x_{H_2O}^{sat} = \frac{P_{H_2O}^{sat}}{P} \quad (9)$$

The molar fraction of N_2 is calculated as (Eq. 10-12):

$$x_{N_2}^{channel} = \frac{\left(Y_{N_2}^{in} - Y_{N_2}^{out}\right)}{\ln\left(\frac{Y_{N_2}^{in}}{Y_{N_2}^{out}}\right)} \quad (10)$$

where

$$Y_{N_2}^{out} = \frac{1 - x_{H_2O}^{sat}}{1 + \left(\frac{\lambda_{air} - 1}{\lambda_{air}}\right)\left(\frac{0.21}{0.79}\right)} \quad (11)$$

$$Y_{N_2}^{in} = 0.79\left(1 - x_{H_2O}^{sat}\right) \quad (12)$$

In equations 11 and 12, $Y_{N_2}^{in}$ and $Y_{N_2}^{out}$ are the proportion of N_2 moles at the entrance and outlet. In addition, λ_{air} denotes the stoichiometric rate of air.

To determine the actual voltage, we may write (Eq. 13):

$$V_{FC} = E_{Ner} - V_{act} - V_{conc} - V_{ohm} \quad (13)$$

where V_{act}, $V_{conc,}$ and V_{ohm} are activation overpotential, concentration overpotential, and ohmic overpotential (Eq. 13). The activation overpotential can be represented by (Eq.14):

$$V_{act} = -\xi T_{FC} + 0.000193T_{FC}\left(\ln\left(C_{O_2}\right)\right) - 0.000076T_{FC}\ln\left(I\right) + 0.948 \quad (14)$$

C_{O_2} is the concentration of O_2 on the cathode side (Eq. 14). ξ is then defined by (Eq. 15):

$$\xi = 0.0002\ln\left(A_{cell}\right) + 0.000043\ln\left(C_{H_2}\right) + 0.00286 \tag{15}$$

in which, A_{cell} is the active surface and C_{H_2} is the hydrogen concentration at the anode side at equation 15. In addition, these concentrations are defined by (Eq. 16,17):

$$C_{H_2} = 9.174\times10^{-7}\,\mathrm{e}^{\left(\frac{-77}{T_{FC}}\right)} P_{H_2} \tag{16}$$

$$C_{O_2} = 1.97\times10^{-7}\,\mathrm{e}^{\left(\frac{498}{T_{FC}}\right)} P_{O_2} \tag{17}$$

The ohmic overpotential is given by (Eq. 18):

$$V_{ohm} = \frac{IL}{A_{cell}}\left(\frac{181.6\left(1.0+0.03I+0.062\left(\frac{T_{FC}}{303}\right)^2 I^{2.5}\right)}{\left(\zeta-0.643-3I\right)\mathrm{e}^{\left(4.18\left(\frac{T_{FC}-303}{T_{FC}}\right)\right)}}\right) \tag{18}$$

The concentration overpotential is then defined as (Eq. 19):

$$V_{conc} = \frac{RT_{FC}}{n_e F}\ln\left(\frac{I_L}{I_L - I}\right) \tag{19}$$

These overpotentials can be estimated using the relations provided in the literature. Other useful relations of the PEMFC needed for the simulation of this component can be found in the literature. Input data required for modeling PEMFC are given in Ref. [45].

2.2.1.2. PVT cells

Table 1 shows the important relations of PVT cells that need to be considered for a reliable simulation. Further relations can be found in the literature [46,47].

Table 1. Governing equations of PV cells [54]

Energy equations	**Input variables**
$P_{PEME} = Q_{PV}\eta_{PV}$	$T_{ref}=T_0$
$Q_{con}= hA\,(T_g-T_a) + hA\,(T_{ins}-T_a)$	$T_{Sky}=0.0552T_a^{15}$
$Q_{rad}= \sigma\varepsilon A\,[(T_g^4-T_a^4)+(T_{ins}^4-T_{Sky}^4)]$	$h= 2.8+3u_{Wind}$
$Q_{PV}=AG- Q_{con}- Q_{rad}$	$u_{Wind}=2m/s,\ T_a=T_0$

2.2.1.3. PEME

The electrolysis energy is given by (Eq. 20):

$$\Delta H = \Delta G + T\Delta S \tag{20}$$

$T\Delta S$is the energy required for PEME.

The hydrogen flow rate leaving the PEME is mentioned in equation 21 [48]:

$$\dot{N}_{H_2,out} = \frac{J}{2F} = \dot{N}_{H_2O,reacted} \tag{21}$$

J denotes current density and $\dot{N}_{H_2O,reacted}$ refer to the amount of water contributed to the reaction (Eq. 21). The total required energy for PEME is calculated by (Eq. 22):

$$E_{electric} = JV \tag{22}$$

The actual voltage of the PEME can be written as (Eq. 23)

$$V = V_0 + \eta_{act,a} + \eta_{act,c} + \eta_{ohm} \tag{23}$$

V_0 denotes the reversible potential (Eq. 24):

$$V_0 = 1.229 - 8.5 \times 10^{-4}(T_{PEM} - 298) \tag{24}$$

Also, In combination formula [43]:

$$\sigma\big(\lambda(x_m)\big) = [0.5139\lambda(x_m) - 0.326]exp\left[1268\left(\frac{1}{303} - \frac{1}{T}\right)\right] \tag{25}$$

where $x_m$and $\lambda(x_m)$ represent the membrane depth and the H_2O content at the position of xm in equation 25. Also, λxm calculated by (Eq. 26):

$$\lambda(x_m) = \frac{\lambda_a - \lambda_c}{L} x_m + \lambda_c \tag{26}$$

$$R_{PEM} = \int_0^L \frac{dx_m}{\sigma[\lambda(x_m)]} \tag{25}$$

The ohmic overpotential is then defined by (Eq.28):

$$\eta_{ohm} = JR_{PEM} \tag{26}$$

The activation overpotential for the anode and the cathode electrode is explained in equation 29 [44]:

$$\eta_{act,i} = \frac{RT}{F} sinh^{-1}\left(\frac{J}{2J_{0,i}}\right) = \frac{RT}{F} ln\left[\frac{J}{2J_{0,i}} + \sqrt{\left(\frac{J}{2J_{0,i}}\right)^2 + 1}\right] \tag{27}$$

PEME exchange current density is then given by (Eq. 30) [44]:

$$J_{0,i} = J_i^{ref} exp\left(-\frac{E_i^{act}}{RT}\right) \tag{28}$$

WhereE_i^{act} is the activation energy for the anode and cathode also J_i^{ref} is the pre-exponential factor in equation 30. Input values required for the modeling of PEMEs have been given in Ref. [44].

2.2.1.4. Direct Contact Membrane Distillation

The temperature gradient between the feed and permeate interface creates the steam pressure difference. The difference is the driving force to transfer steam through the membrane pores to condense on the cold side. For the simulation of the Direct Contact Membrane Distillation (DCMD) system, the mass flux should be considered. Mass flux inside the MD system could be written as follows (Eq. 31) [49]:

$$J_w = C_m(P_1 - P_2) \tag{29}$$

where C_m indicates membrane coefficient. P_1 and P_2 denote the vapor pressures of steam at the membrane layers with a temperature of T_{hm} and T_{cm} (Eq. 31). The vapor pressure (in Pa) is defined by (Eq. 31,32):

$$P_1 = \mathrm{e}^{\left(23.238 - \frac{3841}{T_{hm}-45}\right)}\left(1 - C_s\right)\left(1 - 0.5C_s - 10C_s^2\right) \tag{30}$$

$$P_2 = \mathrm{e}^{\left(23.238 - \frac{3841}{T_{cm}-45}\right)} \tag{31}$$

in equation 32 C_s and C_m are the salinity of water entering the membrane in percentage and the permeability of the membrane respectively and can be calculated according to three different regions[50]. Knudson flow mechanism (Eq. 34):

$$C_m^k = \frac{2\varepsilon r}{3\tau\delta}\left(\frac{8M_w}{\pi RT}\right)^{\frac{1}{2}} \tag{32}$$

Molecular diffusion mechanism (Eq. 35):

$$C_m^d = \frac{\varepsilon}{\tau\delta}\frac{M_w PD}{P_a RT} \tag{33}$$

Knudson-molecular diffusion transition mechanism (Eq. 36):

$$C_c^m = \left[\frac{1.5\tau\delta}{\varepsilon r}\left(\frac{\pi RT}{8M_w}\right)^{\frac{1}{2}} + \frac{\tau\delta}{r}\frac{P_a}{PD}\frac{RT}{M_w}\right]^{-1} \tag{34}$$

where T is the average membrane temperature ($T=(T_{hm}+T_{cm})/2$).

The flow mechanisms through the pores of the membrane can then be given using the Knudsen number:

$kn < 0.01$ Molecular diffusion

$0.01 < kn < 1$ Knudsen-Molecular diffusion transition mechanism

$kn > 1$ Knudsen mechanism

The kn can be calculated by (Eq. 37) [49]:

$$kn = \frac{S}{d} \tag{35}$$

where d is the mean pore diameter of the membrane and S denotes the mean free path of the transferred gas molecule. Also, S is defined as (Eq. 38) [49]:

$$S = \frac{k_B T}{\sqrt{2}\pi P d_e^2} \tag{36}$$

considering the heat transfer from feed toward membrane surface, feed heat flux is defined by (Eq. 39):

$$q_f = h_f \left(T_h - T_{hm}\right) \tag{37}$$

heat flux through the membrane is (Eq. 40):

$$q_m = J_w H_v + h_m \left(T_{hm} - T_{cm}\right) \tag{38}$$

according to equation 40, $H_v(T)$denotes the enthalpy of vaporization of water at mean temperature T:

$$H_v(T) = -1.6\times10^{-3}T^2 + 2.8273T + 1850.7 \tag{39}$$

furthermore, the conduction heat loss of the membrane can be obtained by (Eq. 42):

$$h_m = \frac{k_m}{\delta_m} \tag{40}$$

heat transfer from the permeate side to the water through the convection is given by (Eq. 43):

$$q_p = h_p \left(T_{cm} - T_c\right) \tag{41}$$

considering the steady-state condition in equation 44, we have:

$$q_f = q_m = q_p \tag{42}$$

the overall coefficient of heat transfer is defined as (Eq. 45):

$$U = \frac{1}{\frac{1}{h_p} + \frac{1}{h_m + \frac{J_w H_v}{T_{hm} - T_{cm}}} + \frac{1}{h_f}} \tag{43}$$

so, the overall heat transfer via the membrane is given by (Eq. 46):

$$q_t = U \left(T_h - T_c\right) \tag{44}$$

taking into account the macroscopic scale of membrane distillation, the energy balance gives the following equation (Eq. 47):

$$UA\left(T_h - T_c\right) = m_c C_{P_c} \left(T_{c,out} - T_{c,in}\right) \tag{45}$$

C_{p_c} is the heat capacity and m_c denotes the mass of cold water in equation 47. Similarly, the heat balance for the hot side can be written as (Eq. 48):

$$UA\left(T_h - T_c\right) = m_{hin} C_{P_h} \left(T_{h,in} - T_{h,out}\right) \tag{46}$$

also $m_{h,out}$ obtianed from the following mass balance (Eq. 49):

$$m_{h,in} - m_{h,out} = m_w \tag{47}$$

m_w is calculated by using the mass flux (J_w). Modeling flowcharts of the whole system and the MD system are provided in Figures 2 and 3.

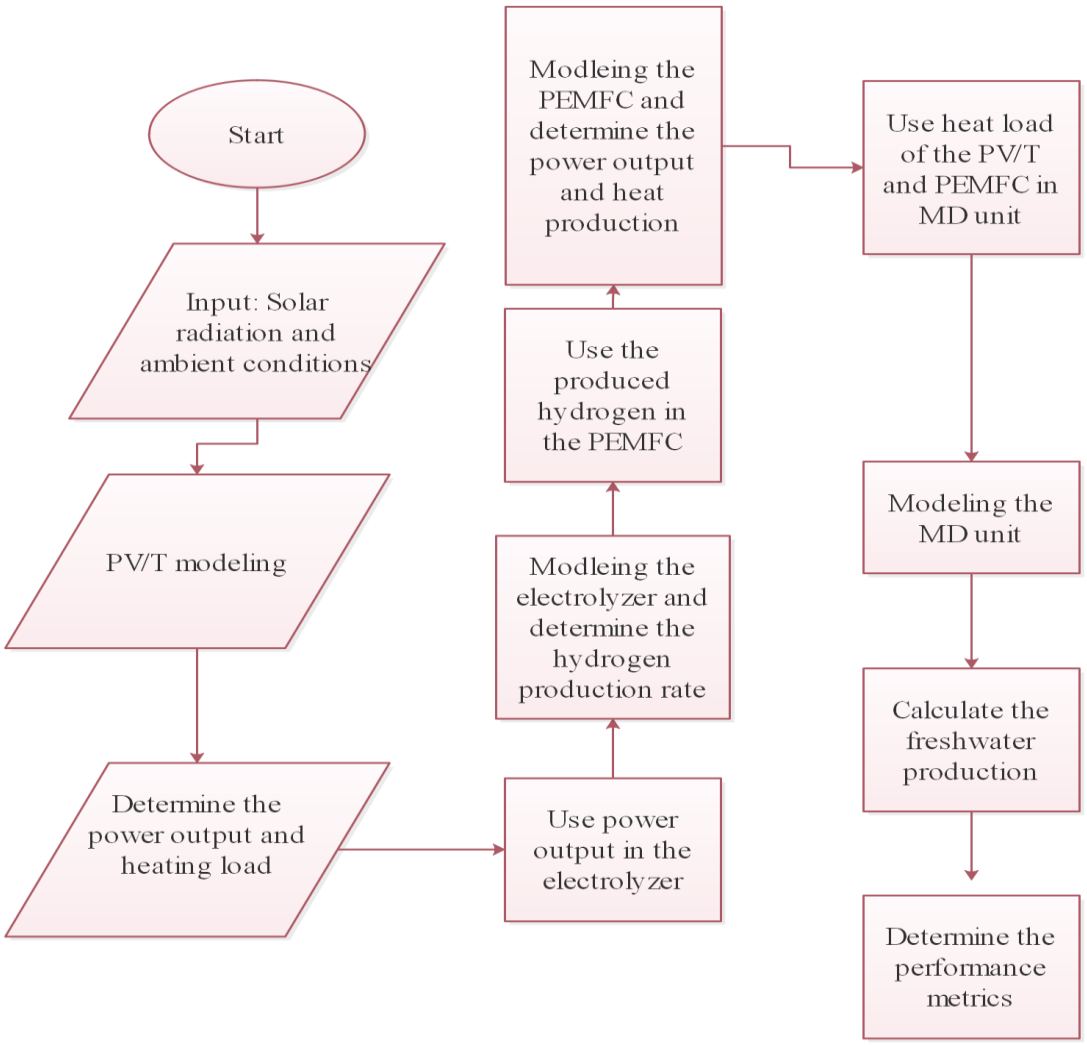

Figure 2. Modeling flowchart of the whole system

It should be noted that multiplying J_w by effective surface area of the membrane concludes the mass flow rate of the distilled water. MD system can be simulated using some input values that can be found in the literature [49]. The input values applied for the simulation are provided in Table 2.

2.2.2. Exergy analysis

Following the second law definition, exergy analysis is helpful to determine the irreversibilities within the system. The exergy of stream material is divided into two parts as defined in (Eq. 50):

$$\dot{E}x = \dot{E}x_{ph} + \dot{E}x_{ch} \tag{48}$$

physical and chemical exergies can be written by (Eq. 51,52) [51]:

$$\dot{E}x_{ph} = \sum_i \dot{n}_i[(h_i - h_0) - T_0(s_i - s_0)] \tag{49}$$

$$\dot{E}x_{ch} = \sum_i \dot{n}_i \sum_i \left(x_i ex_{ch,i} + \bar{R}T_0 x_i . lnx_i\right) \quad (50)$$

the irreversibility caused by each component is then given by (Eq. 53):

$$\dot{E}x_D = \sum \dot{E}x_{in} - \sum \dot{E}x_{out} \quad (51)$$

the rate of input solar energy into the proposed system is calculated by (Eq. 54)[52]:

$$\dot{E}_s = A_r F_R (S - \frac{A_r}{A_a} U_L (T_{in} - T_0)) \quad (54)$$

here, A_r is the collector's receiver area, F_R is considered as removal factor, A_a is the aperture area, U_L illustrates the overall heat loss coefficient related to the solar collector and S indicates the absorbed heat by the receiver (Eq. 54). Moreover, the input exergy that is reached by the solar collector is measured by (Eq. 55) [52]:

$$\dot{E}x_s = A_{coll} G_t [1 + \frac{1}{3}\left(\frac{T_0}{T_s}\right)^4 - \frac{4}{3}\left(\frac{T_0}{T_s}\right)] \quad (55)$$

where, $A_{coll}$is the collector's area,$G_t$is the instantaneous solar radiation, and $T_s$is the temperature of the sun's surface (Eq. 55).

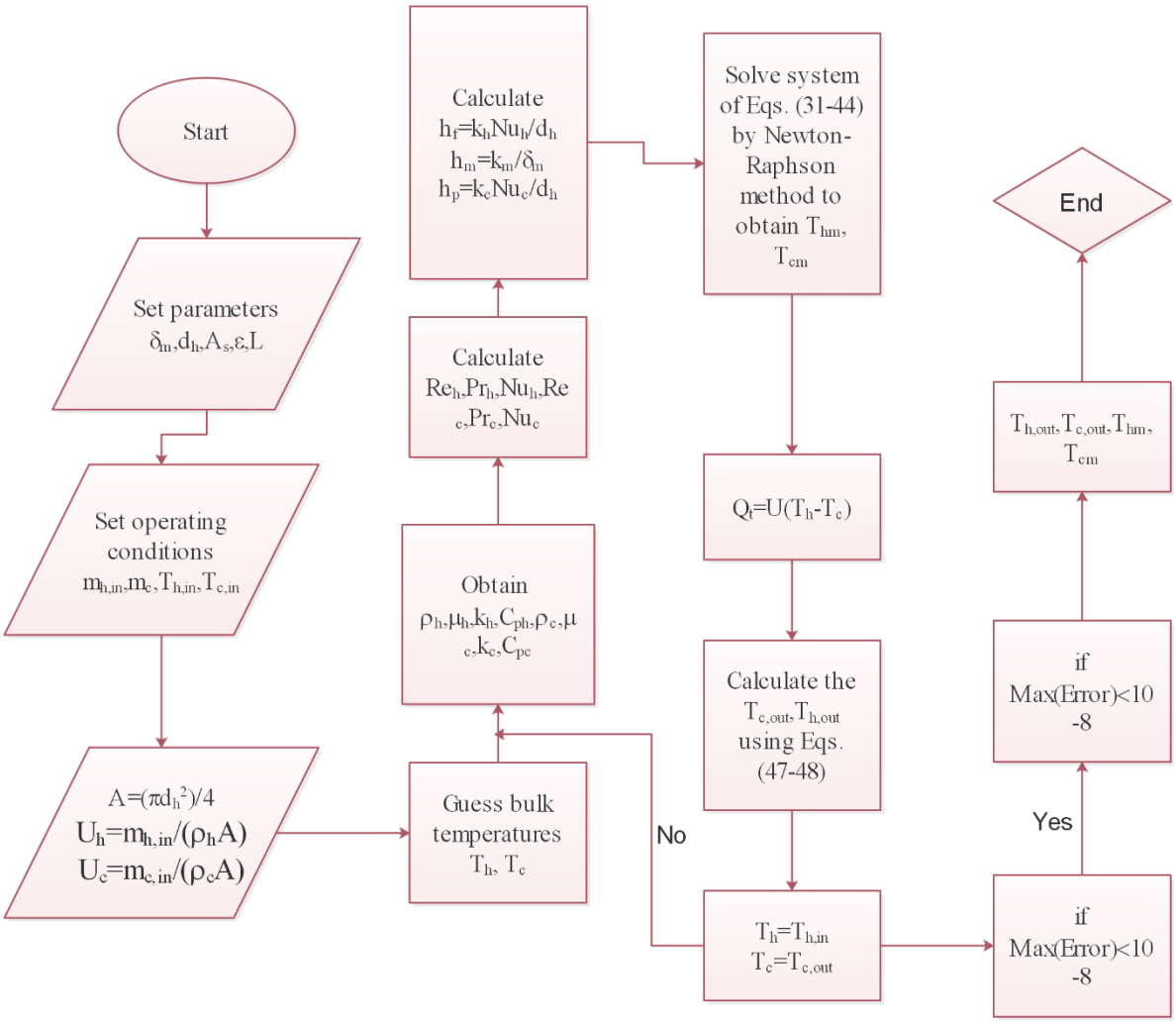

Figure 3. Modeling flowchart of the MD system

Table 2. Input data for the simulation

Variable	Value	Variable	Value
PEME		***PEMFC***	
T_{PEME}	80 °C	T_{stack}	70 °C
E_a^{act}	76 kJ/mol	A_{PEMFC}	232 cm^2
E_c^{act}	18 kJ/mol	λ_{air}	2
λ_a	14	λ_{H2}	1.2
λ_c	10	HHV_{H2}	285.55 kJ/mol
J	500 mA/cm^2	I	100 mA/cm^2
J_a^{ref}	1.7×10^3 A/m^2	n_e	2
J_c^{ref}	$4.6\times10^5 A/m^2$	***MD unit***	
PVT		ε	0.85
		δ	4.5×10^{-5}m
β	0.004 C^{-1}	r	0.22×10^{-6}m
u_{wind}	2 m/s	d_h	4 mm
T_0	25 °C	A	0.0572 m^2
G	800 W/m^2	$T_{h,in}$	70 °C
T_{PV}	70 °C	$T_{c,in}$	C 20

2.2.3. Multi-objective optimization

Some objective functions that are usually in direct competition are considered the target functions –also called objective functions. Objective functions are optimized at the same time to extract a set of solutions with respect to optimum points. Optimization can be conducted using various algorithms while the genetic algorithm has always been a good choice because of its noteworthy advantages for the energy systems [53]. The Matlab toolbox of genetic algorithm is used to conduct the optimization. The genetic algorithm is used to optimize the system and a similar approach is taken into account as described in Ref. [42]. The population size of 100 beside 10 generations, probability of crossover and mutation of 85% and 1% are respectively considered. The values of inputs and target functions will be given with respect to different optimum solutions.

2.2.4. Performance criteria

Some performance criteria are considered to examine the proposed system from various aspects. The first law of the system efficiencies is defined as (Eq. 56):

$$\eta_{th} = \frac{P_{tot} + \dot{m}_{H_2} \times LHV_{H_2}}{\dot{Q}_{sol}} \tag{56}$$

where $\dot{m}_{H_2}$ the excessive hydrogen is produced and $\dot{Q}_{sol}$ is the received heat by the solar collector. In addition, the freshwater mass flow rate and exergy efficiency of the proposed system is given by (Eq. 57):

$$\dot{m}_{freshwater} = J_W \times A_{MD} \tag{57}$$

$$\eta_{ex} = \frac{\dot{m}_{H_2} \times e_{H_2}^{ch} + P_{tot} + \dot{E}_{freshwater}}{\dot{E}_{sol}} \tag{58}$$

where A_{MD} is the effective surface area of the membrane and J_w is the mass flux of the freshwater, $e_{H_2}^{ch}$ is the hydrogen chemical exergy and $\dot{E}_{freshwater}$ is the exergy of freshwater, and $\dot{E}_{sol}$ is the exergy of the solar energy received by the collector. Net power output is obtained as follows (Eq. 59):

$$P_{tot} = P_{PVT} - P_{PEME} + P_{PEMFC} \tag{59}$$

energy utilization factor can also be written as (Eq. 60):

$$\varsigma = \frac{\dot{m}_{w,tot} \times \Delta H_v + P_{tot} + \dot{m}_{H_2} \times LHV_{H_2}}{\dot{Q}_{sol}} \tag{60}$$

where $\dot{m}_{w,tot}$ is the mass flow rate of the produced fresh water, ΔH_v is the vaporization enthalpy and LHV denotes to the lower heating value.

3. RESULTS AND DISCUSSION

3.1.Validation

Firstly, simulation of each subsystem is validated by considering the reported data in the previous works. The validation of the electrolyzer, PEMFC, PVT cells, and MD system are provided in Figure 4, Table 3 to Table 5, respectively. A maximum error of 9% is seen in the simulation of MD.

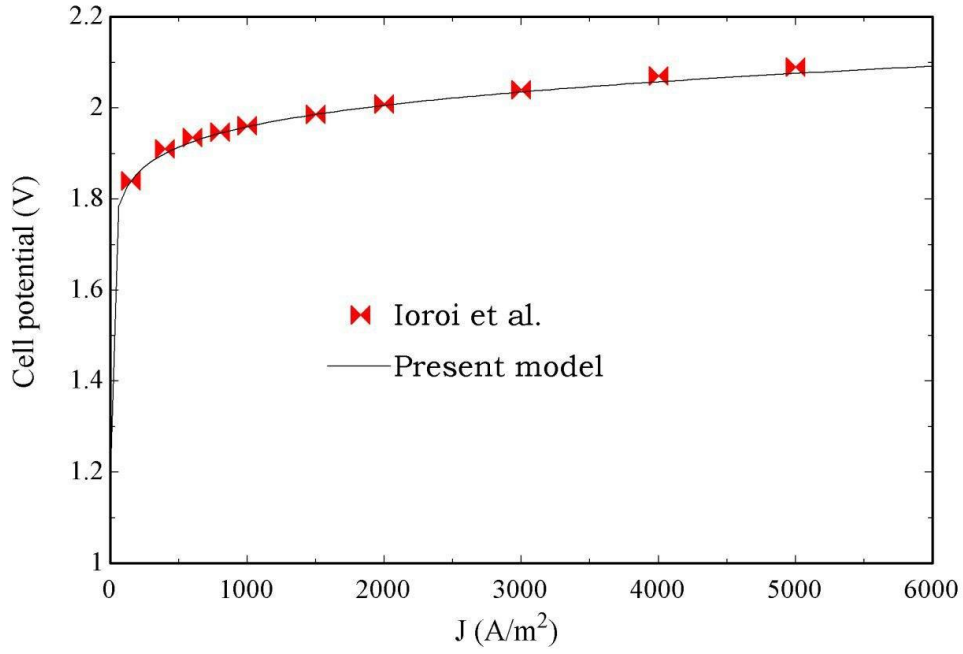

Figure 4. Validation of PEME [56]

Table 3. Validation of PEMFC

Inlet gas temperature (K)	Cell voltage (V)	Cell voltage (V) [55]	Deviation (V)
348	0.675	0.656	0.019
353	0.684	0.678	0.006
358	0.692	0.691	0.001

Table 4. Validation of PVT system

Concentration ratio	Present study Power (kW)	Ref. [54]; Power (kW)	Deviation (kW)
2	0.128	0.127	0.001
5	0.321	0.318	0.003
10	0.643	0.635	0.008
15	0.964	0.953	0.011
20	1.285	1.272	0.013
40	2.570	2.598	-0.028
60	3.856	3.898	-0.042
100	6.426	6.498	-0.072

Table 5. Validation of MD system considering different inlet temperature of warm water

T_{hin} (^{o}C)	J_w(kg/(m^{2}s))(modeling)	J_w(kg/(m^{2}s))[50]	Deviation (%)
80	0.0023	0.0024	4.1
70	0.0016	0.0017	5.8
60	0.0010	0.0011	9.0
50	0.00065	0.0007	7.1
40	0.00034	0.00037	8.1

3.2. Sensitivity analysis

The parametric study provides a helpful method to evaluate the suggested system performance when the inlet parameters are changed. Input parameters are altered, and the influence of them are investigated on the net power generation of the system, the mass flow rate of the distilled water, and exergy and energy efficiencies of the proposed system. The exergy destruction of each component is provided in Figure 5.

3.2.1.The inlet temperature of the MD unit ($T_{h,in}$)

As demonstrated in Figure 6, the impact of the inlet temperature of the MD unit ($T_{h,in}$) on the functionality of the system is assessed. As shown in the mentioned figure, changes in T_{hin} do not have any impact on the total generated power because of the point that this component does not have a contribution to the process of electricity generation. Moreover, by making a change in $T_{hin,}$ the rate of freshwater generation increases.

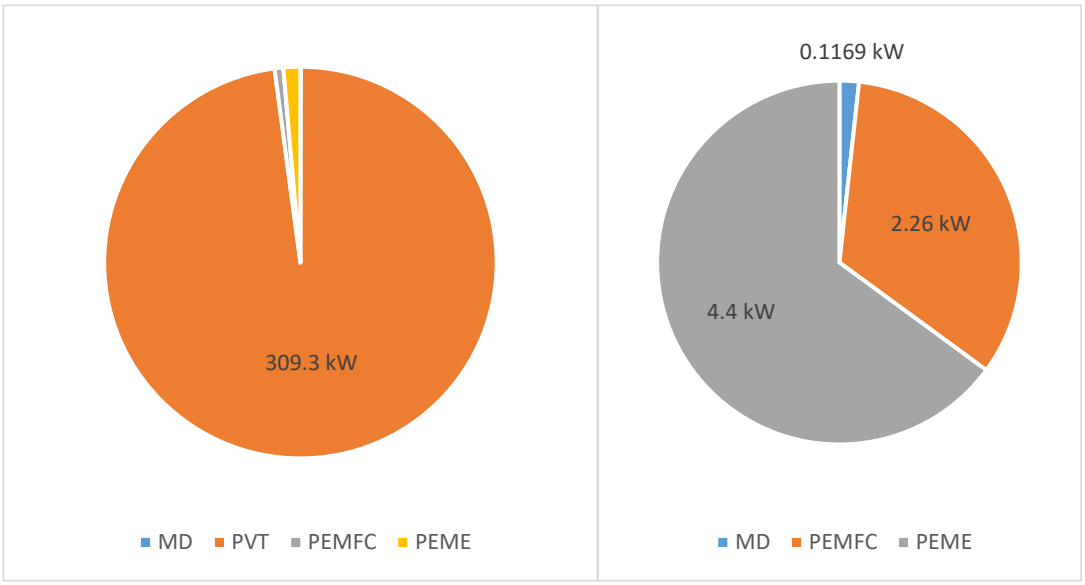

Figure 5. The share of exergy destruction for each component

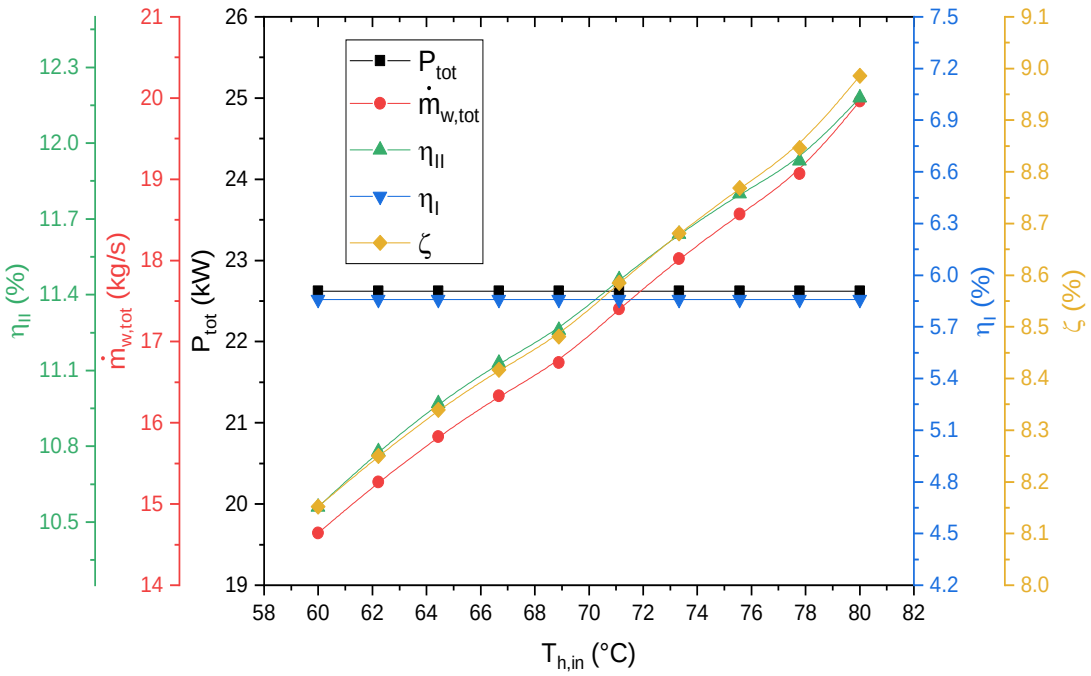

Figure 6. The impact of the hot inlet temperature of the membrane distillation (T_{hin})on the performance criteria of the proposed cycle

The reason for the mentioned improvement is that desalination is contingent on the temperature of the inlet stream and also by increasing the temperature of input salty water, input thermal energy enhances and the rate of the desalinated water improves. The reason is that with increasing the hot water temperature entering the MD unit, the vapor pressure at the feed hot side increases so the pressure difference between the two sides of the membrane increases; consequently, the driven force on vapor from the hot side to the cold side increases,

so higher vapor is turned into freshwater at the cold side. On the other hand, enhancing the production of the system (rate of the desalinated water) has a close relationship with the exergetic efficiency of the system as shown in the related curve, this factor has been improved. Also, the thermal efficiency of the system has not been influenced by T_{hin} due to this parameter does not have any relation to the thermal efficiency of the system. With increasing the inlet temperature, the energy utilization factor increases due to the increased freshwater production.

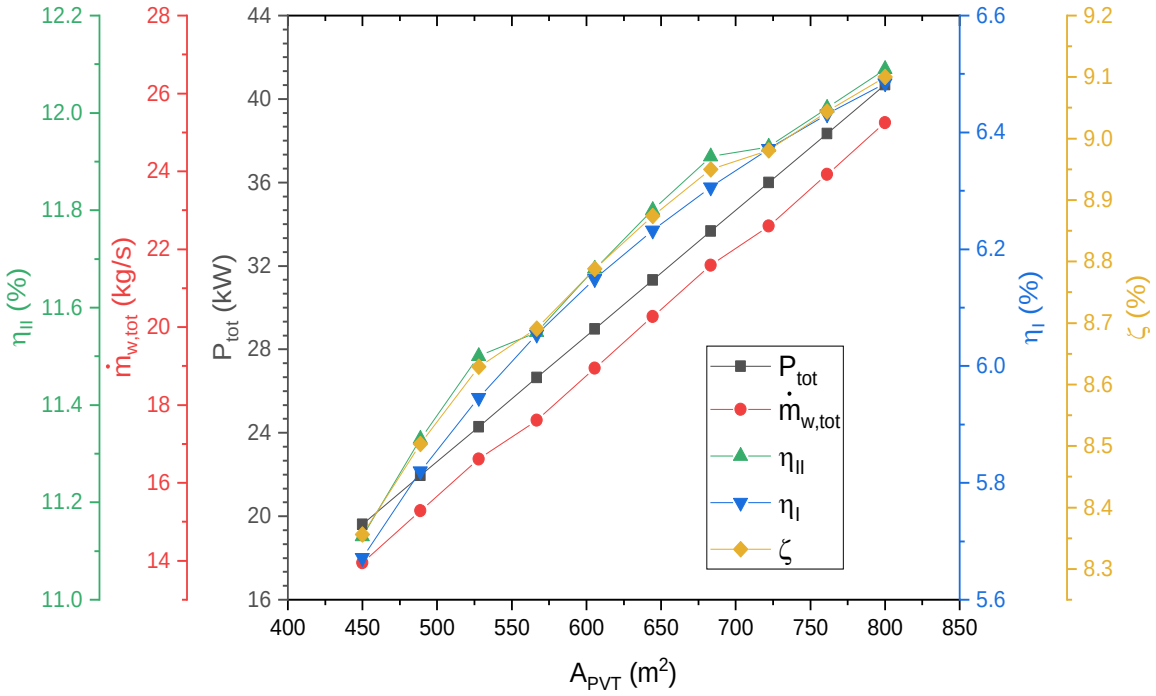

Figure 7. The impact of the area of photovoltaic solar collector (A_{PV})on the functionality of the cycle

3.2.2. The area of photovoltaic solar collector (A_{PV})

As shown in Figure 7, the impact of the area of photovoltaic solar collector (A_{PV}) on the functionality of the hybrid system is evaluated. With raising the A_{PV}, the energy and the exergy efficiencies, the total power generation, and the mass flow rate of the distilled water increased. because of this point, by enhancing the A_{PV} the input heat flux of the system improve and the power generation of the system is enhanced. On the other hand, improving the power generation causes a positive impact on the efficiencies of the plant and as it is crystal clear, all of the curves that are related to efficiencies of the system experience an improvement. In a nutshell, all of the objective functions of the system improve by increasing the A_{PV} factor. Energy utilization factor, similarly to other efficiencies, increases due to the higher freshwater production and power output.

3.2.3. The solar radiation intensity (G)

Alteration of performance metrics of the system influenced by changing the solar radiation intensity has been illustrated in Figure 8. As it is vivid, with raising the *G* value, the energy and the exergy efficiencies of the system increase exponentially by the descent gradients. Also, the rate of water desalination, and power generation increase with linear gradients. The reason that can be highlighted here for mentioned behaviors is that the improvement in solar radiation means an increase in input thermal energy of the proposed system. Consequently, the power and the water generations improved and these enhancements cause an improvement in the efficiencies of the plant. The energy utilization factor is closely related to the other systems' efficiencies. It means higher solar radiation leads to higher power generation and freshwater production.

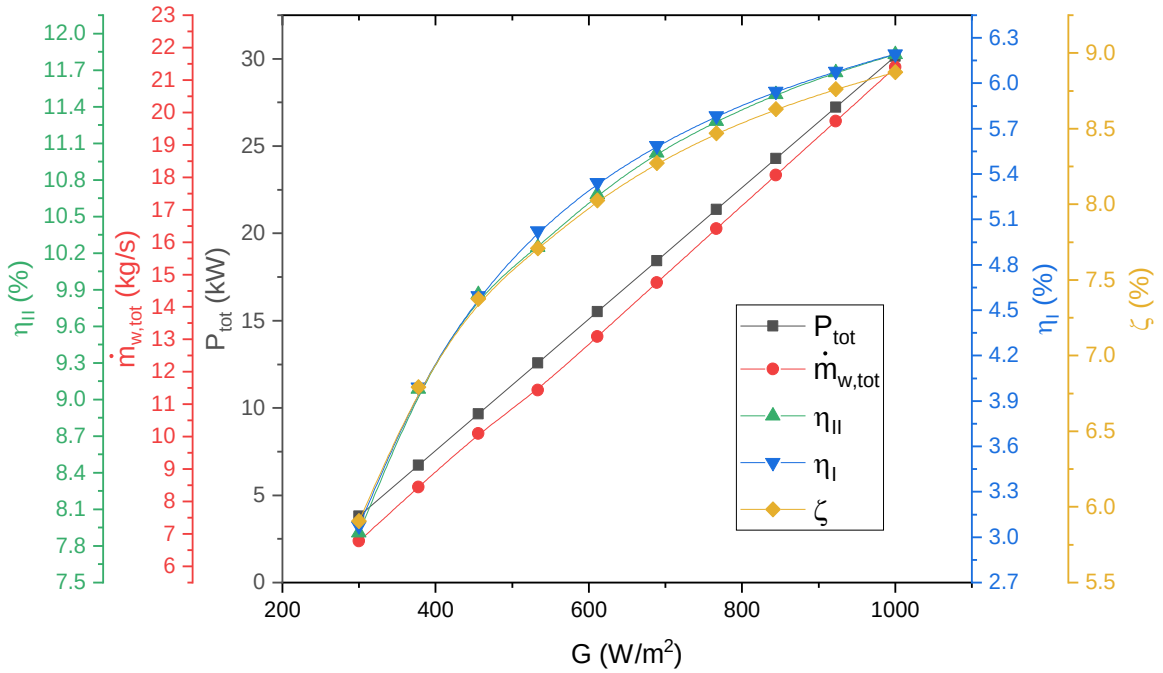

Figure 8. The influence of the solar radiation intensity (*G*)on the performance criteria of the proposed cycle

3.2.4. The current density of the electrolyzer(JPEME)

The impact of the electrolyzer current density (*JPEME*) on the functionality of the system was demonstrated in Figure 9. From the behaviors of the power generation curve of the hybrid system, it can be concluded that by enhancing the *J* factor, the mentioned parameter decreases remarkably. This behavior is because of the point that *J* has a direct relation with the consumed power of the unit and overly the net power generation of the system decreases. Besides, decreasing in the power generation make a decrement in plant efficiency and it is vivid in the figure, mentioned indicators decrease significantly. Furthermore, higher current densities

would lead to higher H_2 consumption, so that higher heat from the PEMFC can be provided for the MD unit, so freshwater production increased.

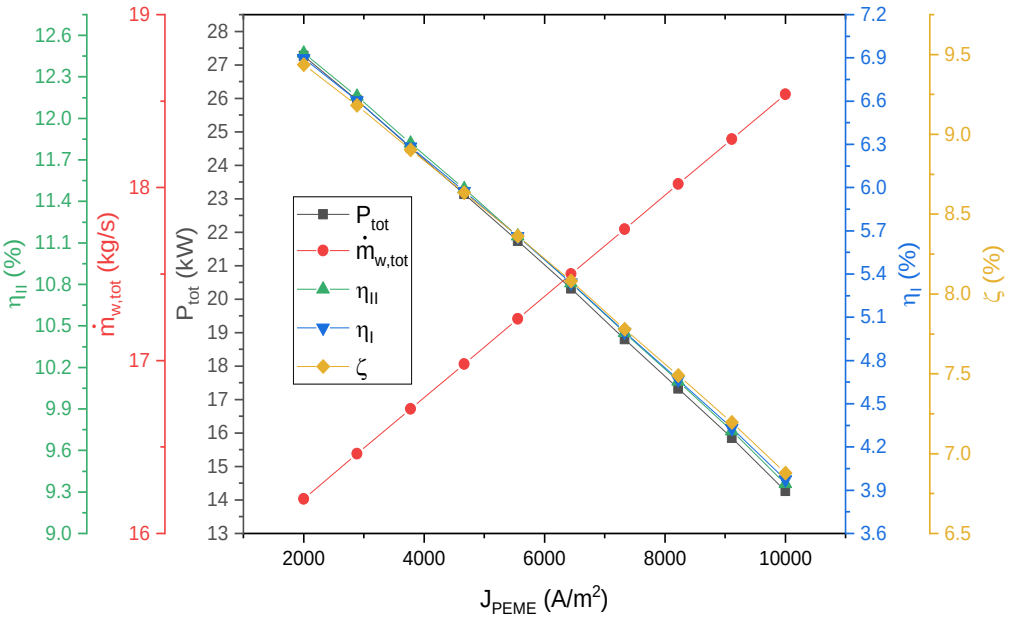

Figure 9. The influenceof the electrolyzer current density (J_{PEME}) on the functionality of the system

3.2.5. The electric current density of the PEMFC (J_{PEMFC})

As shown in Figure 10, the influence of alteration of the electric current density of the fuel cell on the performance criteria of the suggested plant is studied. From the figure, it can be found that, power generation, and efficiencies of the plant decrease when the J_{PEMFC} factor improves. The reason that should be emphasized here is that the energy consumption of the electrolyzer has a direct relationship with the J_{PEMFC} factor and it makes a negative impact on the overall power generation of the unit. This negative impact can be found in the related curve and as it is clear it decreases with a decent gradient. On the other hand, by decreasing the total generation power, the exergetic and thermal efficiencies of the plant decrease. These decrements can be seen in the behaviors of related curves in Figure 10. Besides, changings in the J_{PEMFC} factor increase the freshwater production rate, as higher current densities lead to a higher heat rate available for the MD unit.

3.2.6. The stack temperature of the PEMFC (T_{stack})

Figure 11 depicts the impact of altering the stack temperature of the fuel cell (T_{stack}) on the functionality of the suggested plant. By enhancing T_{stack} factor, the exergetic and thermal efficiencies, and the generation power of the fuel cell unit increase. Furthermore, with increasing the stack temperature, higher heat would be provided for the MD unit, so higher freshwater production is expected.

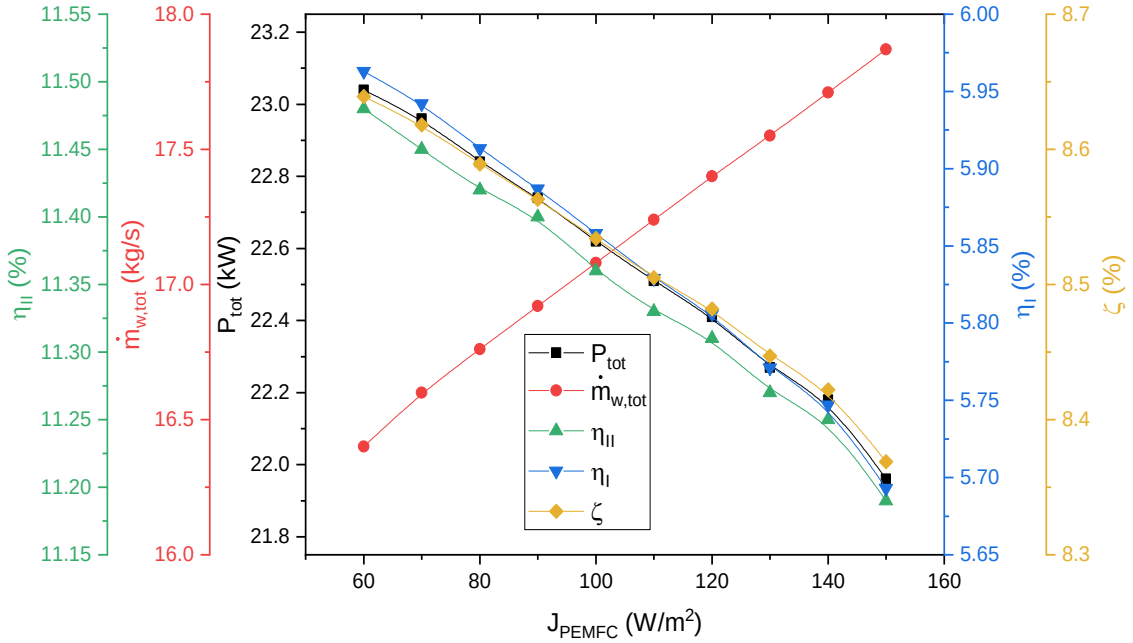

Figure 10. The influence of the PEMF Current density (J_{PEMFC}) on the functionality of the system

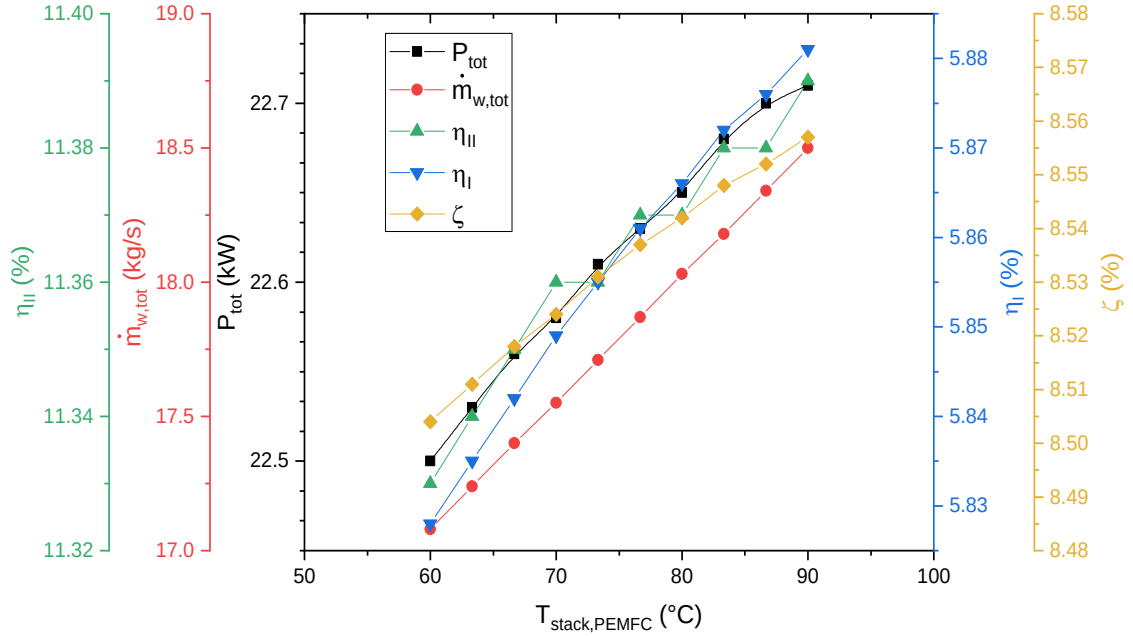

Figure 11. The impact of the PEMFC stack temperature (T_{stack}) on the functionality of the system

3.3. Optimization

The Pareto front consisting of optimum points is demonstrated in Figure 12. As illustrated in the figure, the two conflicting objectives would increase with increasing either of them. Some points are extracted and can be considered for designing the systems depending on the perspective of engineers and stakeholders. However, the desired operating points should be

compared to the ideal solution point shown in the figure. Three different operating points are selected having different efficiency and power. The values of the decision variables that corresponded to these points along with the value of the objective functions are given in Table 6. Point B shows a well-balanced condition between the power and exergy efficiency.

Table 6. Values of decision variables and objective functions at different selected points

Point	Parameters				Objective functions		
	T_{FC}(°C)	J_{PEME} (A/m^2)	I_{FC} (mA/cm^2)	T_{hin}* (°C)	η_{ex} (%)	P (kW)	(kg/h)$\dot{m}_{w,tot}$
A	90	5500	60	70	10.8	40	25.9
B	90	7200	60	75	11.7	30	20.2
C	90	6400	60	78	13	22.5	17.1

*T_{hin} is the hot stream inlet of MD

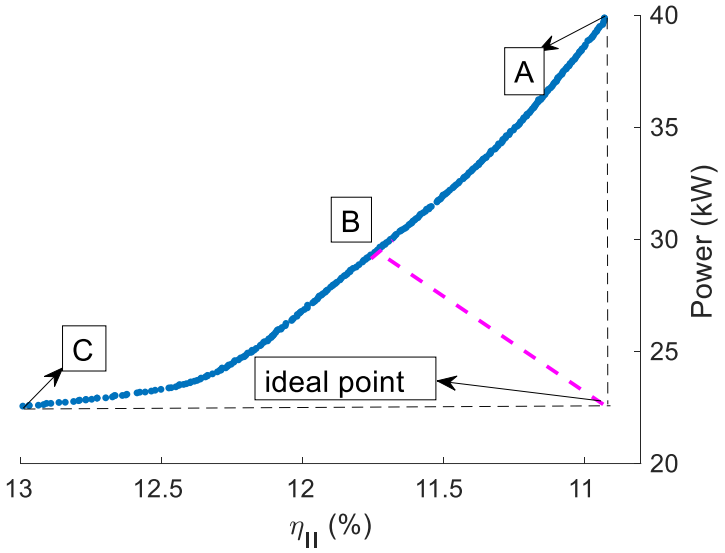

Figure 12. Pareto frontier consisting of optimal solutions

4. CONCLUSIONS

In this study, a novel system is proposed for power and freshwater production consisting of a PVT cell, PEMFC and electrolyzer, and MD system. The required heat of the MD system is provided by PVT cells and PEMFC which also meet the required power of the electrolyzer. The hydrogen produced is transferred to PEMFC for power generation. The proposed system is comprehensively analyzed from a thermodynamics viewpoint and also optimized using multi-objective optimization. The main results of this study are:

- A higher area of PVT cells can increase the power output and freshwater production as the required energy for the MD system improves
- The current density of the electrolyzer and fuel cell is very influential and the fuel cell current density should be kept at lower values to support satisfactory performance

- The inlet temperature of the MD system should be higher to conclude higher freshwater production
- The highest exergy degradation rate belongs to thermal photovoltaic cell (PVT) with 309.3 kW and the lowest exergy degradation rate belongs to the membrane desalination system with 0.11 kW.
- After thermal photovoltaic cell, the highest rate of exergy degradation belongs to the electrolyzer with a value of 4.4 kW, followed by the proton exchange membrane fuel cell with a value of 2.26 kW.
- Increasing the temperature of the fuel cell stack both increases the power production in the fuel cell and also increases the temperature of the water entering the desalination plant and, naturally, increases the fresh water production.
- Changes in the cross section of the solar cell can affect up to 80% and changes in the intensity of solar radiation can affect up to 230% of the fresh water produced.The optimal condition results from multi-objective optimization show efficiency of 11.7%, and 30 kW power.
- The freshwater production rate, following the optimal points determined on the Pareto frontier, will be about 17.1–25.9kg/h.
- The energy utilization factor of the system ranges from 5.5–to 9.5% depending on the operating condition.

REFERENCES

[1] A. I. H. Azeez, B. Deiminiat, G. H. Rounaghi, and S. Kolahi-Ahari, Anal. Bioanal. Electrochem. 14 (2022) 74.
[2] M. A. Sheikh-Mohseni, V. Hassanzadeh, and B. Habibi, Anal. Bioanal. Electrochem. 13 (2021) 214.
[3] P. Kokoskarova, and R. Gulaboski, Anal. Bioanal. Electrochem. 14 (2022) 270.
[4] R. Badrnezhad, and A. F. Zonouz, Anal. Bioanal. Electrochem. 14 (2022) 160.
[5] M. Gökçek, and Ö. B. Gökçek, Desalination 381 (2016) 47.
[6] N. Ghaffour, T.M. Missimer, and G. L. Amy, Desalination 309 (2013) 197.
[7] M. T. Mito, X. Ma, H. Albuflasa, and P. A. Davies, Renew. Sustain. Energy Rev. 112 (2019) 669.
[8] A. Kazim, Energy Convers. Manag. 45 (2004) 1949.
[9] S. Obara, and I. Tanno, Int. J. Hydrogen Energy 33 (2008) 2300.
[10] A. Midilli, and I. Dincer, Int. J. Hydrogen Energy 34 (2009) 3858.
[11] A. Yilanci, I. Dincer, and H. K. Ozturka, Int. J. Hydrogen Energy 33 (2008) 7538.
[12] D. Bezmalinović, F. Barbir, and I. Tolj, Int. J. Hydrogen Energy 38 (2013) 417.
[13] N. Karami, N. Moubayed, and R. Outbib, Energy Convers. Manag. 82 (2014) 154.
[14] M. Hatti, A. Meharrar, and M. Tioursi, Renew. Sustain. Energy Rev. 15 (2011) 5104.

[15] T. J. Leo, J. A. Durango, and E. Navarro, Energy 35 (2010) 1164.
[16] S. Touati, A. Belkaid, R. Benabid, K. Halbaoui, and M. Chelali, Procedia Eng. 33 (2012) 366.
[17] M. M. Sarafraz, M. R. Safaei, A. S. Leon, I. Tlili, T. A. Alkanhal, Z. Tian, M. Goodarzi, and M. Arjomandi, Energy 12 (2019) 2572.
[18] S. D. Farahani, M. Alibeigi, A. Zakinia, and M. Goodarzi, J. Therm. Anal. Calorim. (2021) 1.
[19] M.E. Demir, and I. Dincer, Int. J. Hydrogen Energy 42 (2017) 30044.
[20] E. Baniasadi, S. Toghyani, and E. Afshari, Int. J. Hydrogen Energy 42 (2017) 5327.
[21] H. Rezk, E.T. Sayed, M. Al-Dhaifallah, M. Obaid, A. H. M. El-Sayed, M. A. Abdelkareem, and A. G. Olabi, Energy 175 (2019) 423.
[22] M. Smaoui, and L. Krichen, Control, Energy 114 (2016) 1187.
[23] G. Kyriakarakos, A.I. Dounis, K.G. Arvanitis, and G. Papadakis, Appl. Energy 187 (2017) 575.
[24] D.P. Clarke, Y.M. Al-Abdeli, and G. Kothapalli, Energy 88 (2015) 457.
[25] Z. Li, S. Khanmohammadi, S. Khanmohammadi, A. Al-Rashed, P. Ahmadi, and M. Afrand, Int. J. Hydrogen Energy 45 (2019) 2168.
[26] A. Uzun, B. Bokor, and D. Eryener, Int. J. Hydrogen Energy 45 (2020) 34654.
[27] B. Ghorbani, M. Mehrpooya, and M. Sadeghzadeh, Energy Convers. Manag. 165 (2018) 113.
[28] M. Cilogluları, M. Erden, M. Karakilcik, and I. Dincer, Int. J. Hydrogen Energy 42 (2017) 2547.
[29] D. Ghribi, A. Khelifa, S. Diaf, and M. Belhamel, Int. J. Hydrogen Energy 38 (2013) 8480.
[30] E. Akrami, A. Nemati, H. Nami, and F. Ranjbar, Int. J. Hydrogen Energy 43 (2018) 622.
[31] A. H. Keshavarzzadeh, P. Ahmadi, and M. R. Safaei, Int. J. Hydrogen Energy 44 (2019) 21379.
[32] H. Ishaq, I. Dincer, and G. F. Naterer, Appl. Therm. Eng. 142 (2018) 767.
[33] M. Chahartaghi, and B. A. Kharkeshi, Appl. Therm. Eng. 128 (2018) 805.
[34] M. Shaygan, M. A. Ehyaei, A. Ahmadi, M. E. H. Assad, and J. L. Silveira, J. Clean. Prod. 234 (2019) 1082.
[35] S. Maddah, and M. R. Safaei, J. Therm. Anal. Calorim. 145 (2021) 1537.
[36] R. Dadsetani, G.A. Sheikhzadeh, M. R. Safaei, A. A. Alnaqi, and A. Amiriyoon, Heat Mass Transf. 55 (2019) 1995.
[37] X. Lai, R. Long, Z. Liu, and W. Liu, Energy 147 (2018) 578.
[38] S. Mehrdad, R. Dadsetani, A. Amiriyoon, A. S. Leon, M. R. Safaei, and M. Goodarzi, Process. 8 (2020) 264.

[39] M. M. Sarafraz, M. R. Safaei, A. S. Leon, U. Khaled, M. Goodarzi, and R. Meer, Process. 7 (2019) 763.
[40] A. R. Seifi, O. A. Akbari, A. A. A. A. Alrashed, F. Afshary, G. A. S. Shabani, R. Seifi, M. Goodarzi, and F. Pourfattah, Appl. Therm. Eng. 129 (2018) 1124.
[41] M. R. Qtaishat, and F. Banat, Desalination. 308 (2013) 186.
[42] A. Habibollahzade, E. Gholamian, P. Ahmadi, and A. Behzadi, Multi-criteria, Int. J. Hydrogen Energy 43 (2018) 14140.
[43] A. Habibollahzade, E. Gholamian, E. Houshfar, and A. Behzadi, Energy Convers. Manag. 171 (2018) 1116.
[44] M. Ni, M. K. H. Leung, and D. Y. C. Leung, Energy Convers. Manag. 49 (2008) 2748.
[45] A. H. Keshavarzzadeh, P. Ahmadi, and M. R. Safaei, Int. J. Hydrogen Energy 44 (2019) 21379.
[46] Y. Chen, J. Wang, C. Ma, and Y. Gao, Energy 176 (2019) 479.
[47] A. Habibollahzade, Energy 166 (2019) 118.
[48] A. Habibollahzade, E. Gholamian, P. Ahmadi, and A. Behzadi, Int. J. Hydrogen Energy 43 (2018) 14140.
[49] K. Nakoa, K. Rahaoui, A. Date, and A. Akbarzadeh, Sol. Energy 119 (2015) 319.
[50] K. Nakoa, A. Date, and A. Akbarzadeh, Desalination Water Treat. 56 (2015) 2618.
[51] A. Bejan, G. (George) Tsatsaronis, M. J. Moran, Thermal design and optimization, Wiley (1996).
[52] A. Noorpoor, P. Heidarnejad, N. Hashemian, and A. Ghasemi, Energy Equip. Syst. 4 (2016) 281.
[53] A. Habibollahzade, Energy 166 (2019) 118.
[54] G. Kosmadakis, D. Manolakos, and G. Papadakis, Sol. Energy 85 (2011) 308.
[55] X. Chen, G. Gong, Z. Wan, L. Luo, and J. Wan, Int. J. Hydrogen Energy 40 (2015) 10647.
[56] T. Ioroi, K. Yasuda, Z. Siroma, N. Fujiwara, and Y. Miyazaki. J. Power Sources 112 (2002) 583.